Scale-dependent anisotropy in forced stratified turbulence

C. J. Lang and Michael L. Waite*
Department of Applied Mathematics, University of Waterloo, 200 University Avenue West, Waterloo, Ontario, N2L 3G1, Canada

(Received 10 October 2018; published 3 April 2019)

In stratified turbulence, buoyancy forces inhibit vertical motion and lead to anisotropy over a wide range of length scales, which is characterized by layerwise pancake vortices, thin regions of strong shear, and patches of small-scale turbulence. It has long been known that stratified turbulence becomes increasingly isotropic as one moves to smaller length scales, as the eddy timescale decreases towards and below the buoyancy period. This paper investigates the anisotropy of stratified turbulence across scales and the transition towards isotropy at small scales, using a variety of techniques. Direct numerical simulations of strongly stratified turbulence, with buoyancy Reynolds numbers Re_b up to 50, are analyzed. We examine the relative contributions of different components of the strain rate tensor to the kinetic energy dissipation, the invariants of the isotropy tensor, directional kinetic energy spectra, and the subfilter energy flux across different length scales. At small scales, the degree of isotropy is determined by Re_b, while at the Ozmidov and larger scales, the anisotropy also depends on the Froude number. The change in the anisotropy with scale and with the parameters is examined in detail. Interestingly, Ozmidov-scale eddies are found to become increasingly isotropic as Re_b increases, as characterized by the isotropy tensor invariants and the subfilter energy flux. At larger scales, the energy spectra for near-vertical wave vectors have a spectral slope around -3, which shallow towards -1 for near-horizontal wave vectors. These spectra converge beyond the Ozmidov scale, increasingly so for large Re_b. These results suggest that $\mathrm{Re}_b \gtrsim 500$ would be necessary to obtain the same degree of small-scale isotropy that is found in similarly sized simulations of unstratified turbulence.

DOI: 10.1103/PhysRevFluids.4.044801

I. INTRODUCTION

Stratified turbulence is inherently anisotropic. Gravity, background density stratification, and shear contribute to the breakdown of isotropy and the distinction between horizontal and vertical gradients and velocity components. Under strong stratification, buoyancy forces inhibit vertical motion, reduce the vertical scale of turbulent eddies, and lead to distinct anisotropic modes of motion, including vortical modes and gravity waves [1–3]. Stratified turbulence in the atmosphere and ocean occurs at intermediate and small scales, which are large enough to be influenced by stratification but small enough to not be strongly affected by Coriolis forces [4]. Homogeneous stratified turbulence with vortical mode forcing or initial conditions is commonly used as an idealized model for geophysical turbulence in this regime [5–10]. In this paper, we consider the anisotropy across different scales of stratified turbulence forced by vortical motion. We focus in particular on the large scales, the Ozmidov scale, and the dissipation scale.

*mwaite@uwaterloo.ca

The anisotropy of stratified turbulence varies across length scales. In turbulence dominated by vortical motion, the largest scale eddies are characterized by thin layers of quasihorizontal rotational velocities separated by regions of strong vertical shear. These structures are sometimes called pancake vortices [1]. The limiting behavior for strong stratification at fixed Reynolds number is layerwise two-dimensional turbulence [11–13]. When viscous effects are weak, the thickness of these layers is determined by the buoyancy wave number $k_b \equiv N/U$, where N is the buoyancy frequency and U is the RMS velocity [7–9,14,15], and the layers are separated by regions of Kelvin-Helmholtz instability and small-scale turbulence [16,17]. The large-scale aspect ratio is therefore proportional to the horizontal Froude number

$$\frac{H}{L} \sim \frac{U}{NL} \equiv \mathrm{Fr}_h, \tag{1}$$

where H and L are the vertical and horizontal length scales, and is small in strongly stratified turbulence [14]. The associated vertical velocities are weak [18,19]. The energy cascade to small scales includes anisotropic nonlocal transfers from large horizontal and small vertical scales directly to more isotropic motions around the buoyancy scale [17,20]. When viscous effects are stronger, pancake vortices are viscously coupled in the vertical, and the instabilities and transition to small-scale turbulence are suppressed [9,16,21].

The anisotropy of large-scale vortical motion extends to smaller length scales in stratified turbulence. This anisotropy is characterized by different kinetic energy spectra in the horizontal and vertical wave numbers. Down to the buoyancy wave number, the horizontal wave-number spectral slope is approximately $-5/3$ and the vertical wave-number spectrum is relatively flat [7–9,15,19,22]. At the buoyancy wave number, the horizontal wave-number spectrum sometimes exhibits a bump associated with Kelvin-Helmholtz instabilities between the pancake vortices [9,16,17], while the vertical wave-number spectral slope steepens to around -3 [9,15]. Directional spectra, in which the energy spectra are computed along different angles from the horizontal, also show steeper spectra for more vertical wave vectors [23].

At sufficiently small scales, stratified turbulence starts to resemble isotropic three-dimensional turbulence. This transition happens around the Ozmidov wave number [24,25]

$$k_O \equiv \left(\frac{N^3}{\epsilon}\right)^{1/2}, \tag{2}$$

where ϵ is the kinetic energy dissipation rate. (No factor of 2π is included in the definition of the Ozmidov and other characteristic wave numbers [24,26–28].) At the Ozmidov wave number, the wave-number-dependent eddy frequency $(k_O^2\epsilon)^{1/3}$ is equal to the buoyancy frequency N. Below the Ozmidov scale, eddies evolve more quickly than the buoyancy period; when this timescale separation is large enough, i.e., at sufficiently small scales, the eddies are expected to evolve without being influenced by the stratification. If the Reynolds number is sufficiently large, the horizontal and vertical wave number energy spectra exhibit a $-5/3$ power law between the Ozmidov and Kolmogorov dissipation wave number [22,26,29,30]

$$k_d \equiv \left(\frac{\epsilon}{\nu^3}\right)^{1/4}. \tag{3}$$

The length of the inertial range between k_O and k_d is given by

$$\frac{k_d}{k_O} = \mathrm{Re}_b^{3/4}, \tag{4}$$

where

$$\mathrm{Re}_b \equiv \frac{\epsilon}{\nu N^2} \tag{5}$$

is the buoyancy Reynolds number [27,31]. When L is related to ϵ using Taylor's relation [8] $L \sim U^3/\epsilon$, then $\mathrm{Re}_b \sim \mathrm{Fr}_h^2\mathrm{Re}$, where $\mathrm{Re} \equiv UL/\nu$ is the large-scale Reynolds number. (Note, however, that Taylor's relation may not always be appropriate in stratified turbulence [15,32].) Similarly, the length of the stratified inertial range between the energy-containing wave number $k_i \equiv 1/L$ and k_O is [9]

$$\frac{k_O}{k_i} = \left(\frac{L^2N^3}{\epsilon}\right) \sim \mathrm{Fr}_h^{-3/2}. \tag{6}$$

Therefore, stratified turbulence with a long stratified inertial range (between k_i and k_O) and long small-scale inertial range (between k_O and k_d) requires small Fr_h and large Re_b, and therefore very large Re. Minimum Re_b values required for a fully developed small-scale inertial range have been quoted at from 30 [33] to 200 [27].

At the smallest scales, where viscous dissipation occurs, anisotropy can be quantified by comparing the contributions to the total dissipation. This can be done by comparing the overall contributions from horizontal and vertical gradients [7,22] or by considering the different components of the velocity gradient or strain rate tensors [34–36]. In geophysical or laboratory turbulence, ϵ is often inferred from measurements of a small number of velocity gradients, so knowledge of the ratios of the individual components to the total is important. Dissipation scale isotropy, as described by these ratios, appears to be entirely determined by Re_b [37]. When $\mathrm{Re}_b \lesssim O(1)$, layerwise vortical motion is viscously coupled in the vertical, there is no inertial range below the Ozmidov scale, and the dissipation is dominated by vertical gradients and is therefore very anisotropic [34,38–40]. For increasing $\mathrm{Re}_b \gtrsim O(1)$, the vertical shear contribution to the dissipation decreases and the other components increase, and the dissipation approaches isotropy [9,36,37]. In direct numerical simulation (DNS) studies of homogeneous stratified turbulence without mean shear in which the isotropy of the dissipation components was investigated, Re_b values of up to 14 [36] and 16 [9] were considered. In stratified shear flows, extrapolation of results at lower Re_b suggest that the dissipation would become fully isotropic at $\mathrm{Re}_b \sim 10^5$ [37]; however, without the additional anisotropy of the shear, stratified turbulence without mean shear may isotropize at lower Re_b. Indeed, analysis of PDFs of velocity gradients shows good agreement with isotropic values for $\mathrm{Re}_b \approx 200$ [41].

In this work, we investigate the development of isotropy across scales in stratified turbulence forced by vortical modes over a range of Fr_h, Re, and Re_b. In particular, we focus on the anisotropy of the large scales, associated with the energy-containing vortical modes; the Ozmidov scale, at the scale transition between strongly and weakly stratified eddies; and the small scales associated with energy dissipation. The scaling argument in Eq. (1) suggests that anisotropy of the large scales is determined by Fr_h, while (4) suggests that the isotropy of the dissipation scales is set by Re_b [37]. Such scaling arguments provide a useful guide for thinking about stratified turbulence, but they do not predict how the anisotropy of the turbulence, which can be quantified in various ways, depends on the different parameters. Furthermore, scaling arguments do not predict the anisotropy of eddies at the transition Ozmidov scale. It is not clear how the isotropy of the Ozmidov-scale eddies may depend on Fr_h and Re. Viscous effects at the Ozmidov scale may be important when Re_b is not large enough. These issues are investigated in this work.

Four different anisotropy diagnostics are applied to simulations with Re_b values from 2 to 50, all with very strong stratification. First, the anisotropy of the dissipation tensor is analyzed. While this is a standard approach, we apply it to larger Re_b values than have been considered for homogeneous stratified turbulence without shear. Second, the invariants of the isotropy tensor are considered [42,43]. This approach characterizes the nature of the anisotropy at the energy-containing scales; it has been used in the study of stratified shear flows [37] but not for homogeneous stratified turbulence without shear. We adapt this method, using high-pass filtering, to investigate anisotropy at various length scales. Third, directional kinetic energy spectra are analyzed to determine the degree of isotropy across all length scales over a wider range of parameters than has previously been considered [23,39]. Finally, subfilter-scale energy fluxes [44] are computed and analyzed to

determine the anisotropy of the energy transfer across different length scales. The numerical model is described in the next section. In Sec. III the four anisotropy diagnostics are presented. Results are discussed in Sec. IV, and conclusions are given in Sec. V.

II. NUMERICAL MODEL

Simulations of homogeneous stratified turbulence are performed with a numerical model of the Boussinesq equations

$$\frac{\mathrm{D}\boldsymbol{u}}{\mathrm{D}t} = -\boldsymbol{\nabla} p + b\hat{\boldsymbol{z}} + \boldsymbol{F} + \nu\nabla^2\boldsymbol{u}, \tag{7}$$

$$\frac{\mathrm{D}b}{\mathrm{D}t} + N^2 w = \kappa\nabla^2 b, \tag{8}$$

$$\boldsymbol{\nabla}\cdot\boldsymbol{u} = 0, \tag{9}$$

where $\boldsymbol{u} \equiv (u, v, w)$ is the velocity, p is the pressure scaled by a reference density, b is buoyancy, $\boldsymbol{F}$ is the velocity forcing, N is the constant buoyancy frequency, ν is the kinematic viscosity, and κ is the buoyancy diffusivity. All simulations assume a unit Prandtl number with $\kappa = \nu$.

Equations (7)–(9) are solved with periodic boundary conditions using a Fourier-based spectral transform method. The time-stepping scheme is third-order Adams-Bashforth, with the viscous and diffusive terms handled implicitly with Crank-Nicolson [45]. The number of grid points and wave numbers in each direction is n. The cubic domain has size 2π, yielding integer wave numbers k_x, k_y, k_z. Most aliasing error is eliminated by keeping $8n/9$ wave numbers in each direction and truncating the rest (a ratio of $2/3$ eliminates all aliasing [45], but DNSs have been performed with a ratio as large as $15/16$ [6]). As a result, the maximum effective wave number in each direction is $k_{\max} = 4n/9$ (rounded to the nearest integer), and the effective grid resolution is

$$\Delta x = \frac{9}{8}\frac{L}{n}. \tag{10}$$

The total, horizontal, and vertical magnitudes of wave vectors $\boldsymbol{k} \equiv (k_x, k_y, k_z)$ are denoted by $k \equiv |\boldsymbol{k}|$, $k_h \equiv \sqrt{k_x^2 + k_y^2}$, and $k_v \equiv |k_z|$. The domain-average velocities are zero.

Turbulence is forced by random excitation of large-scale vortical modes [7,8]. Fourier modes with $k \in [3, 5]$ are forced independently with AR(1) red noise. Forcing is centered at $k = 4$, with the amplitude decreasing quadratically to zero at $k = 3$ and 5, as in Ref. [7]. The decorrelation timescale is set to 10 model time steps, so the forcing is effectively white noise [46]. On average, the energy injection rate is approximately equal in all simulations and balances the total dissipation of kinetic and potential energy. Weak damping is applied to the horizontally averaged mean flow (modes with $k_h = 0$) to avoid the slow build-up of energy in the vertically sheared horizontal flow (VSHF), which would otherwise inhibit the development of a stationary state [47–50]. As a result, the kinetic energy in the VSHF saturates at no more than a few percent of the total kinetic energy and does not grow to dominate the flow.

Parameters and some time-integrated quantities are given in Table I. Three stratifications and four viscosities are considered: $N = 0$, 0.15, 0.3, and $\nu = 10^{-5}$, 0.6×10^{-5}, 0.27×10^{-5}, and 0.157×10^{-5}. Time averages are indicated by an overbar. The velocity scale U is calculated as $\overline{E_K}^{1/2}$, where E_K is the domain-average kinetic energy, and L is computed from the time-averaged kinetic energy dissipation rate using Taylor's relation [8] $L \equiv U^3/\bar{\epsilon}$. Note, however, that, by (5), the key parameter Re_b does not depend on how L is computed. Resolutions for the four viscosities are $n = 384$, 576, 1024, and 1536, respectively.

All simulations are initialized with low-level noise at $t = 0$, except for the $n = 1536$ cases, which are initialized with interpolated $n = 1024$ fields with the same N at $t = 450$. Simulations are run to $t = 1000$ time units. The kinetic energy increases until $t \approx 200$, at which time the dissipation

TABLE I. Summary of simulation parameters and time-averaged quantities.

n	N	ν	$k_{\max}$	ϵ	L	U	Fr_h	Re	Re_b	k_b	k_O	$k_{\max}/k_d$	χ_ϵ
384	0	1×10^{-5}	170	2.57×10^{-6}	1.78	0.0166	–	2960	–	0	0	0.754	4.0×10^{-6}
384	0.15	1×10^{-5}	170	1.80×10^{-6}	2.84	0.0172	0.0404	4890	8.00	8.71	43.3	0.825	6.2×10^{-4}
384	0.30	1×10^{-5}	170	1.87×10^{-6}	3.04	0.0178	0.0196	5420	2.07	16.8	120	0.818	4.1×10^{-3}
576	0	0.6×10^{-5}	255	2.53×10^{-6}	1.77	0.0165	–	4850	–	0	0	0.775	2.0×10^{-6}
576	0.15	0.6×10^{-5}	255	1.73×10^{-6}	2.81	0.0169	0.0402	7934	12.8	8.86	44.2	0.853	3.8×10^{-4}
576	0.30	0.6×10^{-5}	255	1.79×10^{-6}	3.01	0.0175	0.0194	8810	3.31	17.1	123	0.845	2.5×10^{-3}
1024	0	0.27×10^{-5}	454	2.66×10^{-6}	1.86	0.0170	–	11 700	–	0	0	0.749	1.4×10^{-6}
1024	0.15	0.27×10^{-5}	454	1.72×10^{-6}	2.95	0.0172	0.0389	18 700	28.3	8.73	44.3	0.835	1.6×10^{-4}
1024	0.30	0.27×10^{-5}	454	1.77×10^{-6}	3.10	0.0176	0.0190	20 200	7.27	17.0	124	0.829	9.1×10^{-4}
1536	0	0.157×10^{-5}	684	1.98×10^{-6}	1.86	0.0154	–	18 300	–	0	0	0.809	8.8×10^{-7}
1536	0.15	0.157×10^{-5}	684	1.84×10^{-6}	3.03	0.0177	0.0390	34 200	52.1	8.46	42.8	0.823	7.8×10^{-5}
1536	0.30	0.157×10^{-5}	684	2.06×10^{-6}	3.30	0.0189	0.0191	39 900	14.6	15.8	114	0.801	3.6×10^{-4}

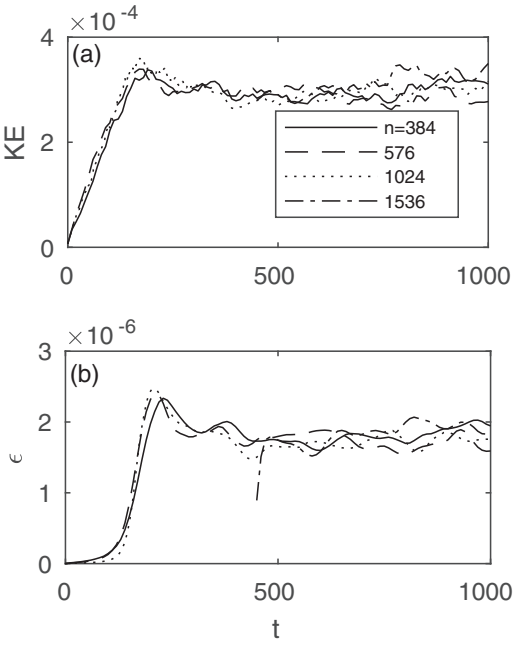

FIG. 1. Time series of (a) kinetic energy and (b) kinetic energy dissipation for simulations with $N = 0.15$ and different n.

reaches a maximum (Fig. 1). Statistical stationarity is reached after a few hundred time units, and various quantities are averaged over $500 \leqslant t \leqslant 1000$. Stratified simulations have $U \approx 0.017$, Fr_h from 0.02 to 0.04, Re from 5000 to 40 000, and Re_b from 2 to 50. All of these simulations can be categorized as strongly stratified (inside the dark gray triangle in the regime diagram by Brethouwer *et al.* [8]); Re_b values are increased by increasing Re, not by weakening the stratification. In all cases, the Kolmogorov scale is resolved with $k_{\max}/k_d \approx 0.8$, and therefore the grid size n is a proxy for Re; we use n values to distinguish simulations with different ν and Re.

The choice of forcing wave number ($k = 4$) is a compromise between competing requirements in DNS of stratified turbulence: the need to minimize domain-size effects, which suggests a large forcing wave number, and the need for large-scale separation between the forcing, Ozmidov, and Kolmogorov scales (small Fr_h and large Re_b), which is facilitated by a small forcing wave number. Our choice of forcing wave number 4 is consistent with other numerical studies of stratified turbulence, which have used both smaller and larger forcing or initial wave numbers. For example, previous DNSs of forced stratified turbulence have forced wave numbers (nondimensionalized for a domain size of 2π) 3 [9], 4 [8], and 5 [22], while studies of decaying stratified turbulence have initialized wave numbers 2 [6], 2.5 [32], 5.6 [19], and 7 [15]. In recent simulations of decaying stratified turbulence [51], the domain size is up to 86 times the initial integral scale, though this ratio decreases as the integral scale grows. We have examined domain-size sensitivity by repeating the simulation with $n = 576$ and $N = 0.15$ with a larger domain size of 4π (effectively forcing wave number 8) and found that the isotropy diagnostics presented below are not significantly affected.

III. QUANTIFYING ANISOTROPY

Four methods are used to quantify the degree and scale dependence of anisotropy in stratified turbulence. Each method is applied to the stratified simulations as well as the unstratified cases, which give a benchmark for the maximum degree of isotropy to expect at a given Re.

A. Dissipation

Evaluation of the relative contributions of the strain rate components to the kinetic energy dissipation is a common approach for evaluating isotropy [34,36] that dates to Taylor [52]. The kinetic energy dissipation rate is given by

$$\epsilon \equiv 2\nu\langle s_{ij}s_{ij}\rangle, \tag{11}$$

where $\langle\cdot\rangle$ is the domain average and s_{ij} is the strain rate tensor. The dissipation is a sum of nine terms ϵ_{ij}, given by the RHS of (11) with no summation. In isotropic turbulence, there are only two different values of ϵ_{ij}, diagonal and off-diagonal, which satisfy [52]

$$\frac{\epsilon_{ij}}{\epsilon} = S_{ij} \equiv \begin{cases} \frac{2}{15} & i = j \\ \frac{1}{10} & i \neq j \end{cases}. \tag{12}$$

Therefore, the degree of isotropy at the dissipation scales can be quantified by comparing the actual values of ϵ_{ij} to their corresponding isotropic values ϵS_{ij}. In addition to considering the individual components of ϵ_{ij}/ϵ, an overall isotropy measure can be obtained from the mean square difference χ_ϵ between the six independent values and their isotropic values. Using time-averaged dissipations, this gives

$$\chi_\epsilon \equiv \frac{1}{6}\sum_{i\geqslant j}(\overline{\epsilon_{ij}/\epsilon} - S_{ij})^2. \tag{13}$$

Small values of χ_ϵ, which is dimensionless, denote greater isotropy at the dissipation scale. For small values of Re_b, ϵ is expected to be dominated by the vertical shear, with [36]

$$\epsilon \approx 2(\epsilon_{13} + \epsilon_{23}). \tag{14}$$

For axisymmetric turbulence, this gives $\chi_\epsilon = 0.0181$. Therefore, stratified turbulence is expected to have $\chi_\epsilon \leqslant 0.0181$, and stratified turbulence with isotropic dissipation scales will have $\chi_\epsilon \ll 0.0181$.

B. Isotropy tensor invariants

A second method for diagnosing isotropy in the velocity field employs invariants of the isotropy tensor [37,42,43]

$$b_{ij} \equiv \frac{\langle u_i u_j\rangle}{\langle u_k u_k\rangle} - \frac{1}{3}\delta_{ij}. \tag{15}$$

This tensor is dimensionless, symmetric, and traceless and vanishes identically in the case of an isotropic Reynolds stress tensor. It has two nontrivial invariants

$$\text{II} \equiv b_{ij}b_{ij}, \quad \text{III} \equiv b_{ij}b_{jk}b_{ki}. \tag{16}$$

The other invariant is the trace, which is always zero. All possible values of II and III must lie inside a triangular region of the II–III plane (the Lumley triangle [42]), two sides of which correspond to axisymmetric turbulence, and one corner of which (II = III = 0) corresponds to isotropic turbulence [see labels in Fig. 5(a) below] [42]. By examining the position of various simulations on the II–III plane, the degree and type of anisotropy can be diagnosed [42,43].

Since b_{ij} is based on the domain-averaged Reynolds stresses, the invariants measure isotropy of the large energy-containing scales [37]. This is in contrast to the dissipation approach, which diagnoses isotropy of the small dissipative scales. However, information about scale-dependent isotropy can be obtained from the invariants by high-pass filtering the velocity fields to remove the largest scales before computing b_{ij}. We employ an isotropic spectral cutoff filter which passes all k larger than the cutoff and completely filters all smaller wave numbers. Two types of cutoffs are considered. First, we remove all $k < 6$, so that the invariants are not contaminated by the

forcing scales, where anisotropy results from the selective forcing of vertical modes and by the relatively small number of Fourier modes. Second, we analyze isotropy at smaller scales relative to the Ozmidov scale by removing all wave numbers with k/k_O below different thresholds (0.25, 0.5, 1, and 1.4). In all cases, invariants are computed from instantaneous velocity fields at $t = 1000$ ($t = 750$ for $n = 1536$, $N = 0.3$).

C. Directional energy spectra

Kinetic energy spectra are computed by summing over spherical shells in wave number space:

$$E(k) \equiv \frac{1}{2} \sum_{\boldsymbol{p} \in S_k} \overline{\hat{u}_i(\boldsymbol{p}, t) \hat{u}_i^*(\boldsymbol{p}, t)}, \tag{17}$$

for integer values of k, where S_k is the spherical shell of radius k and unit width. In Eq. (17), the hat denotes the Fourier coefficient and the star denotes the complex conjugate. In isotropic turbulence, the energy should be uniformly distributed over the spherical shells. However, in anisotropic turbulence the energy distribution may not be uniform, and information about the angular dependence of the energy is lost in the calculation of $E(k)$. A common approach is to separately consider horizontal and vertical wave number spectra by summing over k_v and k_h, respectively. However, more detailed information about anisotropy can be obtained by considering the angular dependence of energy in the S_k [39,53]. We follow the approach of Delache *et al.* [53], who divide the S_k into $2M$ latitude bands $O_{k,i}$ of equal angular width $\Delta\theta \equiv \pi/(2M)$. We use $M = 6$ [53]. Band i corresponds to $|\theta| \in [\theta_{i-1}, \theta_i)$ (vertical wave vectors with $|\theta| = \pi/2$ are included in $O_{k,M}$). The bands are ordered so that $O_{k,1}$ corresponds to nearly horizontal wave vectors with $|\theta| \approx 0$ and $O_{k,M}$ corresponds to nearly vertical wave vectors with $|\theta| \approx \pi/2$ (note, this ordering is opposite to that employed in Ref. [53]). Using weights

$$m_i \equiv \frac{\pi}{4\Delta\theta[\sin(\theta_i) - \sin(\theta_{i-1})]}, \tag{18}$$

which are based on the surface area of the latitude bands, the average energy in each band is

$$E(k, i) \equiv \frac{1}{m_i} \frac{1}{2} \sum_{\boldsymbol{p} \in O_{k,i}} \overline{\hat{u}_i(\boldsymbol{p}, t) \hat{u}_i^*(\boldsymbol{p}, t)}, \tag{19}$$

and the weighted average of the directional spectra gives the total spectrum

$$E(k) = \sum_{i=1}^{M} m_i E(k, i). \tag{20}$$

Because of the normalization, the different directional spectra $E(k, i)$ can be compared directly to evaluate the relative amount of energy in different bands. Isotropic turbulence has $E(k, i)$ independent of i.

The spread in the directional spectra gives a measure of anisotropy at each k. This spread can be quantified by computing the standard deviation of the $E(k, i)$ at each k:

$$\sigma(k) \equiv \left[\frac{\sum_{i=1}^{M} (E(k, i) - \mu(k))^2}{M} \right]^{1/2}, \tag{21}$$

where

$$\mu(k) \equiv \frac{1}{M} \sum_{i=1}^{M} E(k, i) \tag{22}$$

is the average energy across latitude bands [note that, due to the variable weights m_i, $\mu(k) \neq E(k)$]. The standard deviation can be normalized by $\mu(k)$ to give a dimensionless measure of isotropy at

wave number k. Wave numbers with $\sigma(k)/\mu(k) \ll 1$ are isotropic, while those with $\sigma(k)/\mu(k) = O(1)$ have significant anisotropy.

D. Subfilter-scale dissipation

Another scale-dependent measure of isotropy can be obtained by performing an *a priori* analysis of the subfilter-scale energy flux. Let $\widetilde{F}$ denote a low-pass filter of field F. We employ an isotropic spectral cutoff filter which passes all $\boldsymbol{k}$ with $k < k_c$ perfectly and completely filters all larger wave numbers. The rate at which kinetic energy is transferred across k_c from filtered to subfilter scales is [43]

$$\Pi \equiv \langle 2\tau_{ij}\widetilde{s}_{ij}\rangle, \tag{23}$$

where

$$\tau_{ij} \equiv \widetilde{u}_i\widetilde{u}_j - \widetilde{u_iu_j} \tag{24}$$

is the subfilter stress tensor and $\widetilde{s}_{ij}$ is the filtered rate of strain. Note that, while $\tau_{ij}\widetilde{s}_{ij}$ need not be positive at every point in stratified turbulence, and may be negative on a significant fraction of the domain, the domain average Π is positive, as expected for a direct energy cascade [44].

The isotropy of the energy flux Π across k_c can be analyzed in a similar fashion to ϵ. It is the sum of nine terms Π_{ij}, given by the RHS of (23) with no summation. In isotropic turbulence, there are only two different values of Π_{ij}, diagonal and off-diagonal, which satisfy

$$\frac{\Pi_{ij}}{\Pi} = S_{ij} \equiv \begin{cases} \frac{2}{15} & i = j \\ \frac{1}{10} & i \neq j \end{cases}. \tag{25}$$

The derivation of (25) follows Taylor's [52] derivation of (12) and is given in the Appendix. As above, the overall degree of isotropy in Π_{ij} can be obtained from the mean square distance between the six independent values of Π_{ij}/Π and their isotropic values S_{ij}:

$$\chi_\Pi \equiv \frac{1}{6}\sum_{i\geqslant j}(\Pi_{ij}/\Pi - S_{ij})^2. \tag{26}$$

In all cases, Π_{ij} and χ_Π are computed from instantaneous velocity fields at the same times as the invariants.

IV. RESULTS

A. Overview

Snapshots of vertical slices of u are shown in Fig. 2 for $N = 0.15$ and different n. These plots exhibit the familiar pancake structure of stratified turbulence, with the flow organized into vertical layers [5,7,9,29]. In each panel of Fig. 2, there are approximately eight layers visible. Since the buoyancy wave number is $k_b \approx 9$ for $N = 0.15$, the number of layers is consistent with their thickness being equal to the buoyancy scale [7,14]. The large-scale layered structure is insensitive to Reynolds number, but increasing Re leads to more fine-scale structure, and possible regions of small-scale isotropy, which will be explored more below (see the transition from panel a to d in Fig. 2). By contrast, the dependence of the large-scale vertical structure on N is significant (Fig. 3, which shows u for $n = 576$ and different N). In the unstratified case, the wave number 4 forcing is clearly visible, and the velocity field appears isotropic at all scales. However, as N increases, the layered structure emerges and the vertical scale decreases. Furthermore, the small-scale velocity also becomes increasingly anisotropic as N increases, as expected.

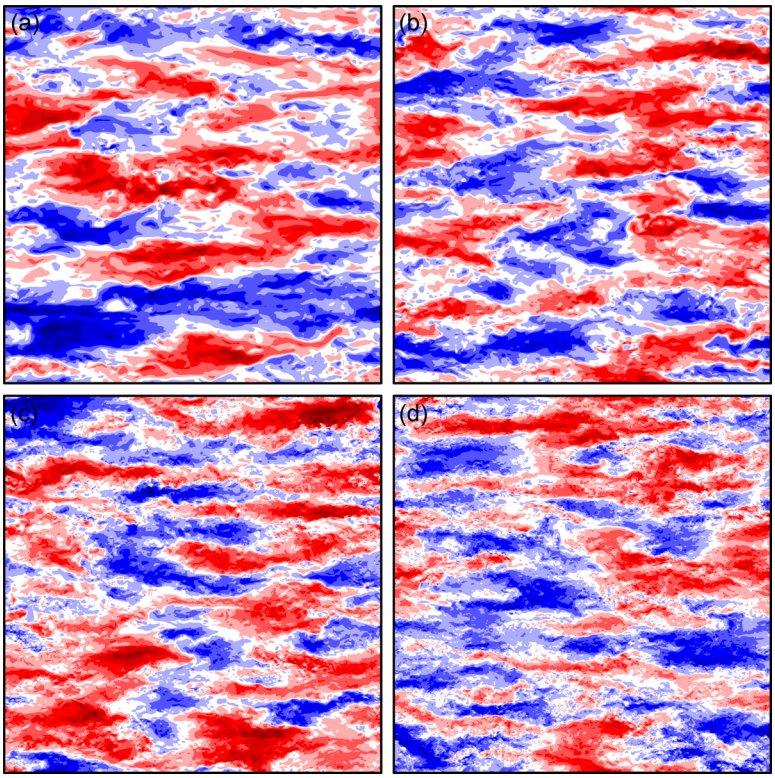

FIG. 2. Vertical (x, z) slices of u at $t = 1000$ for $N = 0.15$ and $n =$ (a) 384, (b) 576, (c) 1024, and (d) 1536. Contour spacing is 0.009.

B. Dissipation

The relative contributions of the different components of the dissipation $\overline{\epsilon_{ij}/\epsilon}$ are plotted against Re_b in Fig. 4(a). At low $\mathrm{Re}_b = O(1)$, the main contributions are from ϵ_{13} and ϵ_{23}, as expected. These components contain the vertical shear, which is known to dominate the dissipation at low $\mathrm{Re}_b \lesssim O(1)$ where the flow is characterized by quasihorizontal pancake vortices [36] [see, e.g., Fig. 3(c), which has $\mathrm{Re}_b = 3$]. As Re_b increases towards 10, ϵ_{13} and ϵ_{23} decrease and the other components increase. Nevertheless, the vertical components ϵ_{13} and ϵ_{23} remain larger, and the horizontal components ϵ_{11}, ϵ_{22}, and ϵ_{12} remain smaller, than their isotropic values, as Ref. [36] found at similar Re_b. Beyond $\mathrm{Re}_b \approx 20$, the components are clearly approaching their isotropic values, although they have still not reached them in any of these simulations. Even at the largest $\mathrm{Re}_b = 50$, which is three times larger than the largest Re_b obtained in Ref. [36], the dissipation is still slightly dominated by the vertical shear.

The overall degree of anisotropy in the dissipation is characterized by χ_ϵ, the mean square difference between the $\overline{\epsilon_{ij}/\epsilon}$ and their isotropic values, which is plotted in Fig. 4(b). This quantity exhibits a clear dependence on Re_b, confirming that the degree of anisotropy in the dissipation is determined Re_b in Ref. [37]. As Re_b increases, the dissipation becomes more isotropic and χ_ϵ decreases. In cases where two simulations have different Fr_h and Re but similar Re_b ($N = 0.15$, $n = 384$ and $N = 0.3$, $n = 1024$, which both have $\mathrm{Re}_b \approx 7$–8, and $N = 0.15$, $n = 576$ and $N = 0.3$, $n = 1536$, which both have $\mathrm{Re}_b \approx 13$–15), the χ_ϵ values collapse well when plotted against Re_b in Fig. 4(b). Indeed, there is an approximately power law relationship between χ_ϵ and Re_b, with $\chi_\epsilon \sim \mathrm{Re}_b^{-1.2}$ [solid curve in Fig. 4(b)]. The largest $\mathrm{Re}_b = 50$ has $\chi_\epsilon = 8 \times 10^{-5}$, which, while small, is still 1–2 orders of magnitude larger than the values with $N = 0$ at all resolutions (Table I). Indeed,

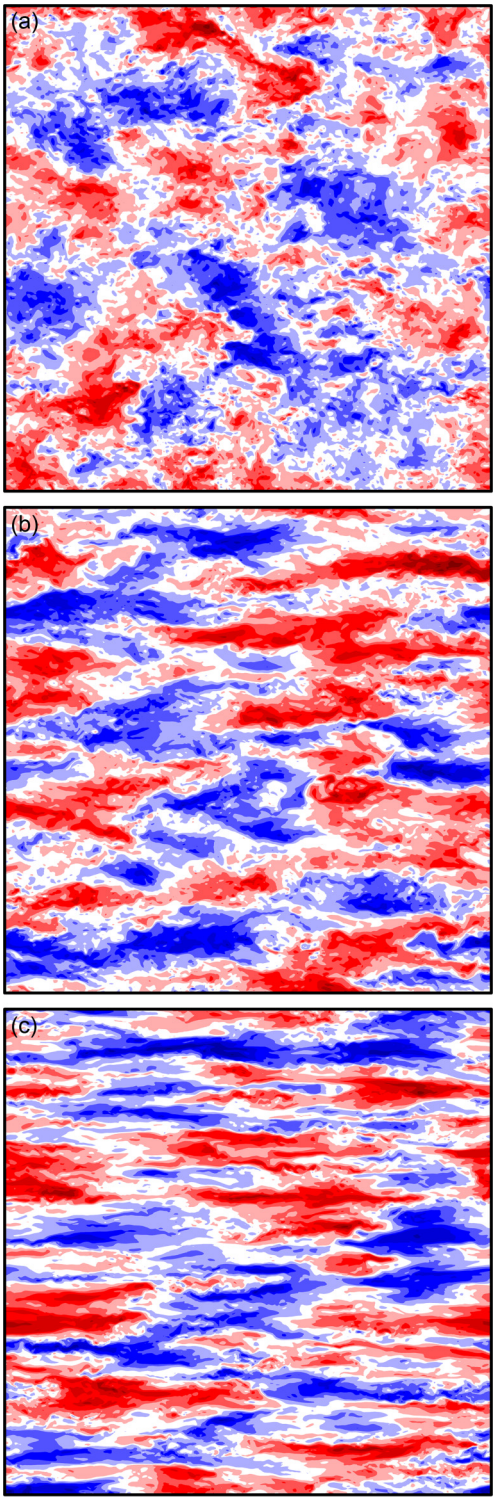

FIG. 3. Vertical (x, z) slices of u at $t = 1000$ for $n = 576$ and $N =$ (a) 0, (b) 0.15, and (c) 0.3. Contour spacing is 0.009.

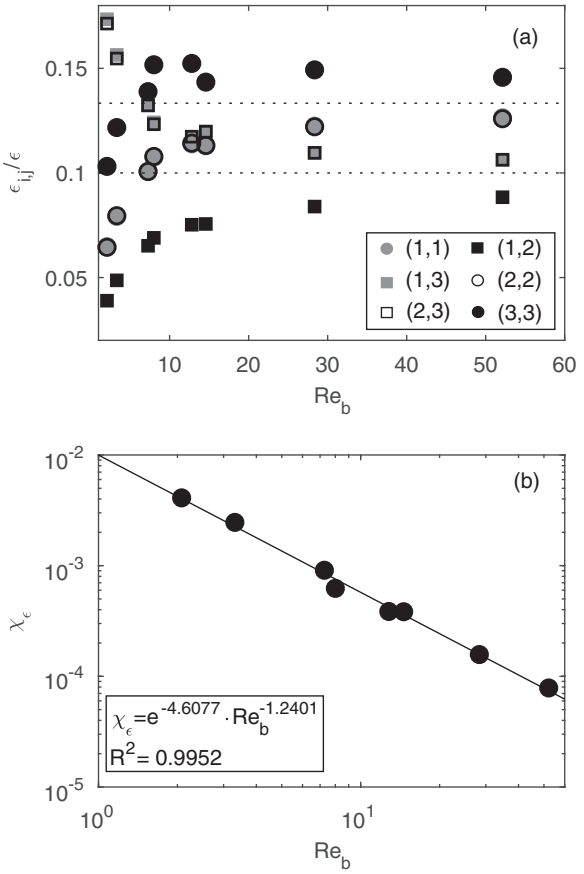

FIG. 4. (a) Relative contribution of different components to the total dissipation $\overline{\epsilon_{ij}/\epsilon}$, and (b) mean square distance χ_ϵ between the $\overline{\epsilon_{ij}/\epsilon}$ and their isotropic values. In panel (a) the isotropic values $1/10$ (for $i \neq j$) and $2/15$ (for $i = j$) are denoted by horizontal lines, and the points for (1,1) and (1,3) are not visible because, due to axisymmetry, they are directly behind the points for (2,2) and (2,3), respectively. In panels (a) and (b), all stratified simulations are included, and values are plotted against Re_b. The solid line shows the power law best fit.

if the power law Re_b dependence in Fig. 4(b) holds at larger Re_b, one would require $\mathrm{Re}_b \approx 550, 960$, 1300, and 1900 to get the same χ_ϵ found in unstratified turbulence at $n = 384, 576, 1024$, and 1536, respectively.

C. Isotropy tensor invariants

Figure 5 shows the isotropy tensor invariants $\amalg$ and $\triangle\!\!\!\triangle$ for all simulations with the forcing scales ($k < 6$) removed. Panel (a) shows the full Lumley triangle, and panel (b) zooms in on the simulation data. All invariants lie on the bottom left side of the triangle, which is axisymmetric and connects two-dimensional and three-dimensional isotropic turbulence. The unstratified simulations lie at the three-dimensional isotropic point $\amalg = \triangle\!\!\!\triangle = 0$, as expected, indicating that there is no significant residual anisotropy from the vortical mode forcing at $k > 6$. The invariants for the stratified simulations are clustered by N, with $\triangle\!\!\!\triangle \approx -0.013$ for $N = 0.3$ and $\triangle\!\!\!\triangle \approx -0.004$ for $N = 0.15$. The invariants approach 0 with increasing Fr_h, indicating an approach to isotropy with decreasing stratification. By contrast, the dependence on Re is much weaker. Since the Reynolds

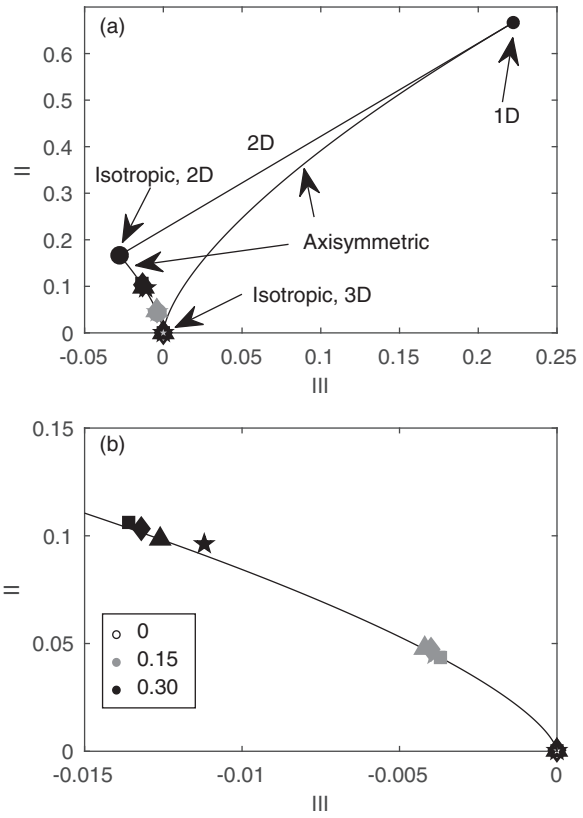

FIG. 5. Isotropy tensor invariants of all simulations. Panel (a) shows the full Lumley triangle, and panel (b) is a zoom on the bottom left side. Shading denotes $N = 0$ (white), 0.15 (gray), and 0.3 (black), and symbols denote $n = 384$ (square), 576 (diamond), 1024 (triangle), and 1536 (star). The triangle boundary and reference points for 1D, isotropic 2D, and isotropic 3D turbulence are also indicated for clarity [43]. Invariants are computed after filtering out the forcing scales $k < 6$.

stresses depend on the velocity components, and the relative size of the large-scale horizontal and vertical velocities in stratified turbulence is determined by Fr_h [1,14], it is natural that Fr_h, not Re, determines the large-scale anisotropy measured by the invariants.

The stratified invariants become increasingly isotropic if the velocity fields are high-pass filtered relative to the Ozmidov scale first. Figure 6 shows the invariants computed after removing scales relative to the Ozmidov scale with $k/k_0 < 0.25$, 0.5, 1, and 1.4 (panels (a)–(d), respectively). Even with the smallest wave number cutoff $k/k_O < 0.25$ ($k < 10$ and $k < 30$ for $N = 0.15$ and 0.3, respectively), the invariants are more isotropic than when only the forcing wave numbers are removed [Fig. 6(a)]. For example, the III values for $N = 0.15$ go from -0.004 to -0.001 as the filter cutoff increases from 6 to $0.25k_O \approx 10$. As more large scales are removed, the invariants move along the axisymmetric blue curve towards $\mathrm{II} = \mathrm{III} = 0$, indicating increasing isotropy at smaller scales. Note the different axis scales in Fig. 6: when velocities are filtered to remove all scales larger than the Ozmidov scale, the largest III are less than 10^{-3} in size [Fig. 6(c)]; if plotted on the original axes in Fig. 5, these points would be almost indistinguishable from 0.

However, despite filtering relative to the Ozmidov scale, the invariants still cluster by N, with the more weakly stratified cases being consistently more isotropic than the stronger stratified cases even with the same k/k_0 cutoff. This is even true for the $n = 384$, $N = 0.15$ case (gray square) and the $n = 1024$, $N = 0.3$ case (black triangle), which have similar $\mathrm{Re}_b \approx 8$: the $N = 0.15$ invariants

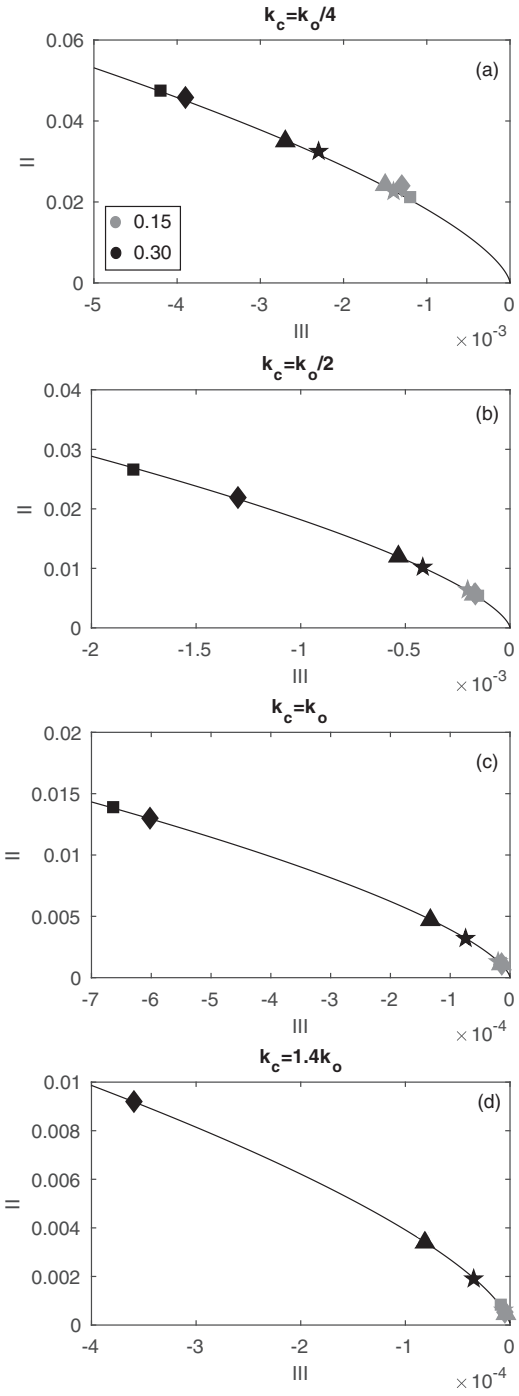

FIG. 6. Invariants after high-pass filtering scales relative to the Ozmidov scale. Invariants are computed after removing (a) $k < 0.25k_O$, (b) $k < 0.5k_O$, (c) $k < k_O$, and (d) $k < 1.4k_O$. Symbols and shading are as in Fig. 5. Note the increase in zoom from panels (a) to (d). In panel (d) the $n = 384$ case with $N = 0.3$ (black square) is not included because $1.4k_O$ is equal to the truncation wave number.

are more isotropic than the $N = 0.3$ invariants at all k/k_0 cutoffs. The same is true for the $n = 576$, $N = 0.15$ (gray diamond) case and the $n = 1536$, $N = 0.3$ case (black star), which have similar $\mathrm{Re}_b \approx 14$. While the Reynolds stresses are clearly more isotropic around the Ozmidov scale than they are at large scales, the degree of isotropy depends on Fr_h independently of Re_b. This behavior is unlike the anisotropy of the dissipation scales considered above, which is entirely determined by Re_b.

In addition, the Ozmidov-filtered invariants exhibit much greater dependence on Re at higher stratifications than lower. The spread in the black points in Fig. 6 is consistently larger than that in the gray points. In all cases, the trend is towards increased isotropy for increasing Re at the same N. Unlike the large-scale isotropy (Fig. 5), the local isotropy around the Ozmidov scale likely depends on Re via Re_b, which gives the width of the inertial range between k_O and k_d [Eq. (4)]. All the simulations with $N = 0.3$ have relatively small $\mathrm{Re}_b \lesssim 10$ and so may depend more on Re than the $N = 0.15$ simulations.

D. Directional energy spectra

Directional kinetic energy spectra for the unstratified simulations are shown in Fig. 7. Outside the forcing range, which is affected by the vortical mode forcing (no direct excitation of w) and the relatively small number of wave vectors at large scales, the simulations exhibit a high degree of isotropy at all resolutions, as expected. The various $E(k, i)$ are close together, with no tendency for energy to accumulate at near-vertical or near-horizontal wave vectors. Beyond $k \approx 20$, the directional spectra are indistinguishable from one another and follow an approximately $-5/3$ slope to k_d. This isotropy is confirmed by considering the standard deviation of the directional spectra, which is shown in Fig. 10(a) below. The normalized standard deviation $\sigma(k)/\mu(k)$ is less than 0.5 at all k and all n. It is smallest in the inertial range, where $\sigma(k)/\mu(k) < 0.1$ and reaches a minimum of 0.04, 0.03, 0.01, and 0.005 for $n = 384$, 576, 1024, and 1536, respectively. The increase in $\sigma(k)/\mu(k)$ at the largest $k \approx k_{\max}$ is due to the rapid decrease of $\mu(k)$ deep inside the dissipation range rather than enhanced anisotropy and will be omitted in the following discussion.

The directional spectra for $N = 0.15$ (Fig. 8) exhibit much greater anisotropy at large and intermediate scales compared to the unstratified simulations. For near-horizontal wave vectors (small i), there is a sharp peak at the forcing wave number $k = 4$; however, moving towards more vertical wave vectors with larger i, the peak broadens, and there is a secondary peak around the buoyancy wave number $k_b \approx 8$. Outside the forcing range, the directional spectra $E(k, i)$ increase with increasing i, indicating that there is greater energy in near-vertical wave vectors than in near-horizontal wave vectors. This angular dependence is characteristic of pancake-like structures [39], e.g., as seen in Fig. 2. The dependence on i is significant: at $k = 10$, just beyond the forcing range and near k_b, there is approximately 50–70 times more energy in $O_{k,6}$ than in $O_{k,1}$, yielding $\sigma(10)/\mu(10) \approx 1.5$ [Fig. 10(b) below]. This large-scale anisotropy does not depend significantly on Re.

Moving to larger k, the spread in the directional spectra narrows because the spectra at large i are steeper than those at small i. For example, for $n = 1536$ [Fig. 8(d)], the spectral slope between $k = 10$ to 40 ranges from -0.98 for near-horizontal wave vectors with $i = 1$ to -2.84 for near-vertical wave numbers with $i = 6$. Slopes at intermediate angles increase with i: slopes are -1.1, -1.3, -1.6, and -2.3 for $i = 2$, 3, 4, and 5. As a result of this steepening, by $k = k_0 \approx 40$ there is only approximately five to six times more energy in $O_{k,6}$ than in $O_{k,1}$. Beyond k_O, the spectra at all i follow an approximately $-5/3$ slope when the inertial range from k_O to k_d is sufficiently long [Fig. 8(d)]. As a result, the standard deviation also decreases with increasing k: $\sigma(k)/\mu(k)$ reaches ≈ 0.7 at $k = k_O$ in all cases with $N = 0.15$ and plateaus at smaller values for larger n, indicating that greater small-scale isotropy, especially in the dissipation range, is reached for higher Re. Nevertheless, even for $n = 1536$, the smallest $\sigma(k)/\mu(k) \approx 0.16$ is 30 times larger than that obtained for $N = 0$ at the same n. The stratified turbulence in this simulation has the largest $\mathrm{Re}_b = 50$ and therefore is expected to have the largest inertial range between the

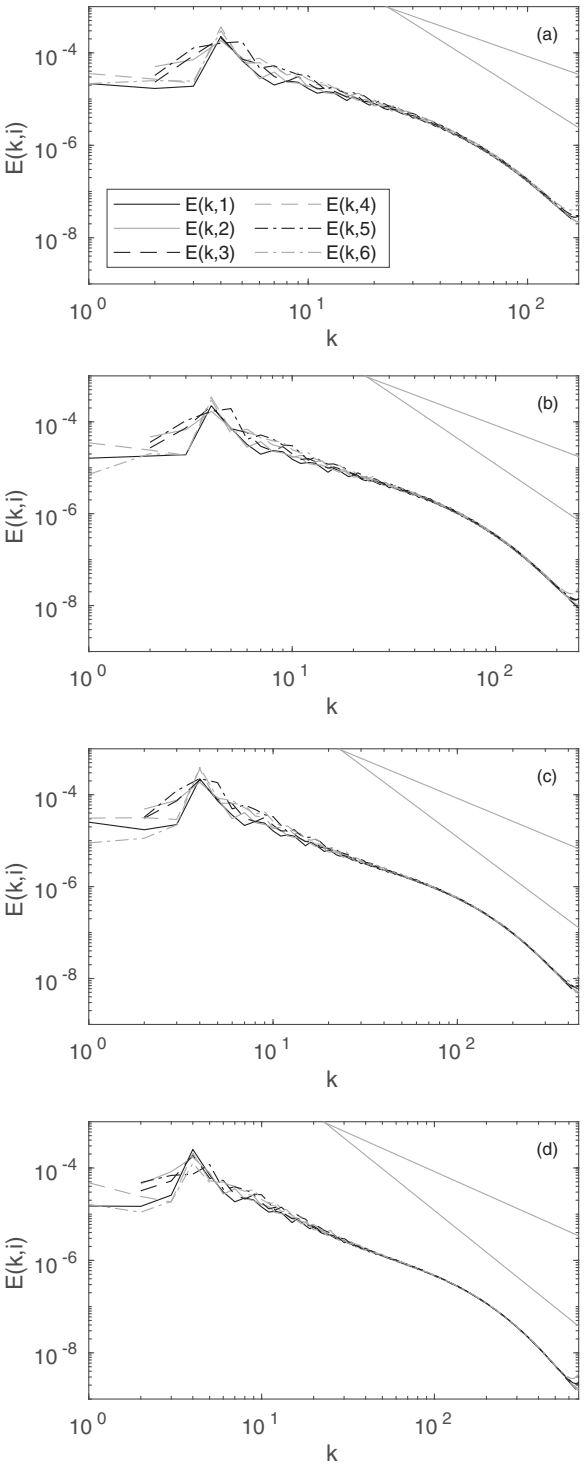

FIG. 7. Directional kinetic energy spectra for $N = 0$ for (a) $n = 384$, (b) 576, (c) 1024, and (d) 1536. The reference lines have slopes of $-5/3$ and -3.

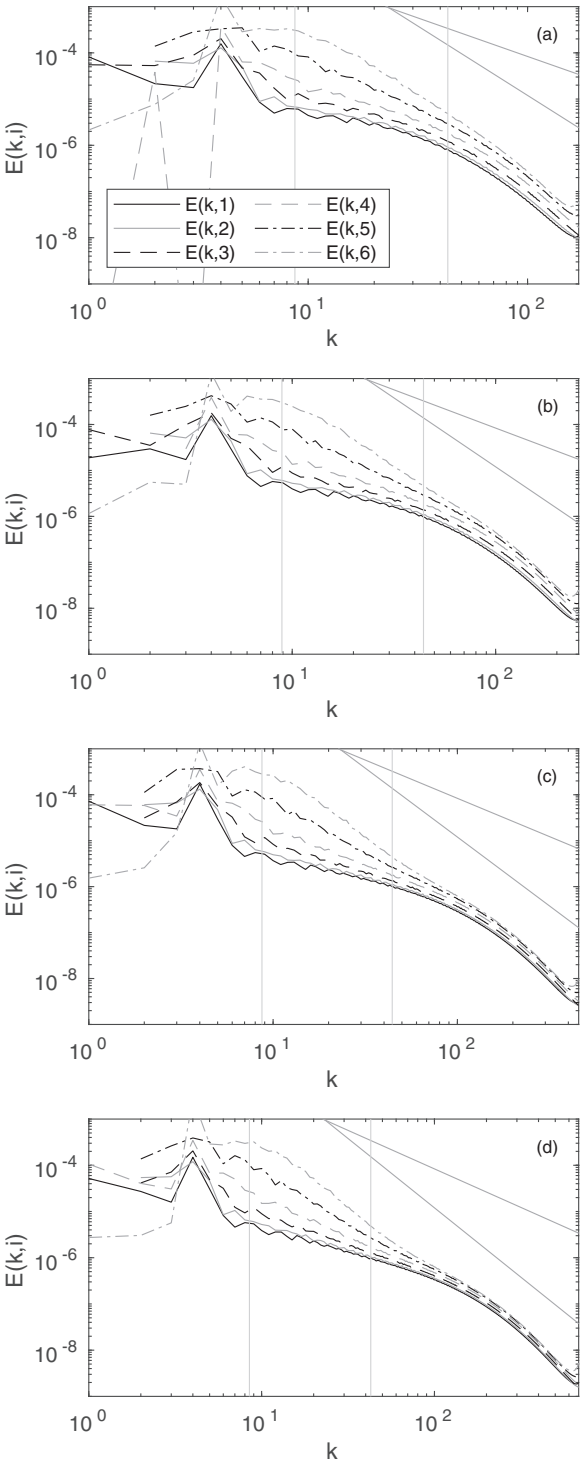

FIG. 8. Directional kinetic energy spectra for $N = 0.15$ for (a) $n = 384$, (b) 576, (c) 1024, and (d) 1536. In all cases, $k_b \approx 9$ and $k_O \approx 43$ are shown with vertical lines. The reference lines have slopes of $-5/3$ and -3.

Ozmidov and Kolmogorov scales; however, the directional spectra at small scales never reach the same degree of isotropy found in unstratified turbulence, even unstratified turbulence with much lower Re.

The directional spectra in the most stratified simulations with $N = 0.30$ (Fig. 9) display even greater anisotropy at all scales. As for $N = 0.15$, there is a preference for energy to accumulate around near-vertical wave numbers with large i, and this preference extends to even larger k than in the $N = 0.15$ simulations. The energy in near-vertical wave numbers continues to show a peak at the buoyancy scale, which is larger at this stratification ($k_b \approx 17$). At $k = 10$, there is approximately 200–300 times more energy in $O_{k,6}$ than in $O_{k,1}$. Again, the spectra at large i are steeper than those at small i: the spectral slopes for $n = 1536$, measured between $k = 20$–40, steepen from -0.66 for $i = 1$ to -2.7 for $i = 6$. By $k = k_O \approx 120$, the ratio of energy in $O_{k,6}$ to $O_{k,1}$ is reduced to from 20 for $n = 384$ to 5 for $n = 1536$. These ratios are generally larger than those obtained at $N = 0.15$ except for the $n = 1536$ case, which is similar. Similarly, the standard deviation $\sigma(k)/\mu(k)$ at $k = k_O$ is more sensitive to n than in the $N = 0.15$ cases and equals 1.1, 0.98, 0.7, and 0.65 for $n = 384$, 576, 1024, and 1536. The isotropy at the Ozmidov scale is sensitive to Re at this stratification, possibly due to the fact that the Re_b values are not too large. While the lower Re simulations have larger $E(k, 6)/E(k, 1)$ and $\sigma(k)/\mu(k)$ at $k = k_O$ than for $N = 0.15$, indicating greater anisotropy at the Ozmidov scale, the ratios and standard deviations in the higher resolution simulations are similar. Beyond the Ozmidov scale, the steep spectra at large i do not have enough room to shallow before reaching the dissipation range, and $\sigma(k)/\mu(k)$ never falls below 0.3 in all simulations with $N = 0.3$.

The nature of the large-scale anisotropy described by $\sigma(k)/\mu(k)$ is different in the unstratified and stratified cases. In the unstratified case, there is a modest degree of anisotropy ($\sigma(k)/\mu(k) \approx 0.5$), mainly around the forcing scales. By contrast, in the stratified cases, the wave number of maximum anisotropy shifts downscale and seems to follow the buoyancy wave number k_b [Figs. 10(b) and 10(c)]. The directional variation in the amount of energy at k_b is greater than at other scales, due to the pancake structure of the large-scale vortices, the thickness of which is given by k_b. The maximum $\sigma(k)/\mu(k)$ increases with increasing stratification, from around 1.5 for $N = 0.15$ to 2 for $N = 0.3$. The maximum values of $\sigma(k)/\mu(k)$ do not depend on Re.

Interestingly, the degree of isotropy in the directional spectra at the Ozmidov scale seems to be largely determined by Re_b, without separate dependence on Fr_h and Re. Consider the simulations with $n = 384$ and $N = 0.15$, and $n = 1024$ and $N = 0.30$, both of which have $\mathrm{Re}_b \approx 8$. The corresponding values of $\sigma(k_O)/\mu(k_O)$ are very similar, at 0.73 and 0.76, respectively [see Figs. 10(b) and 10(c)]. A similar result holds for the simulations with $n = 576$ and $N = 0.15$, and $n = 1536$ and $N = 0.30$, both of which have $\mathrm{Re}_b \approx 14$, and have $\sigma(k_0)/\mu(k_0)$ of 0.67 and 0.65. Similarly, the ratio of Ozmidov-scale energy in the most vertical and horizontal wave-number bands $O_{k,6}$ and $O_{k,1}$ is also a function of Re_b (Fig. 11) and clearly approaches a value between 5 and 6 for $\mathrm{Re}_b \gtrsim 10$. These findings suggest that the isotropy of the total energy distribution in wave vector space at the Ozmidov scale is determined by Re_b. By contrast, the isotropy of the velocity components, as described by the invariants of the isotropy tensor discussed above, are not.

An overall measure of small-scale isotropy is given by the minimum value of $\sigma(k)/\mu(k)$ over k in each simulation. The minimum values generally occur in the dissipation range. The values for the unstratified simulations are 0.041, 0.027, 0.014, and 0.0051 for $n = 384$, 576, 1024, and 1536; these values characterize the maximum amount of isotropy expected at a given n. The values for the stratified simulations are plotted against Re_b in Fig. 12. The data in Fig. 12 collapse well when plotted against Re_b, with an approximate power law of $\sim \mathrm{Re}_b^{-0.57}$; this collapse supports the finding that small-scale isotropy is determined by Re_b. As we did above for χ_ϵ, we can extrapolate this power law to larger Re_b to estimate the Re_b at which the stratified directional spectra exhibit the same degree of small-scale isotropy as the unstratified simulations. This power law suggests that one would require $\mathrm{Re}_b \approx 570$, 1200, 3700, and 21 000 to get the same minimum value of $\sigma(k)/\mu(k)$ found in unstratified turbulence at $n = 384$, 576, 1024, and 1536, respectively. Interestingly, the first

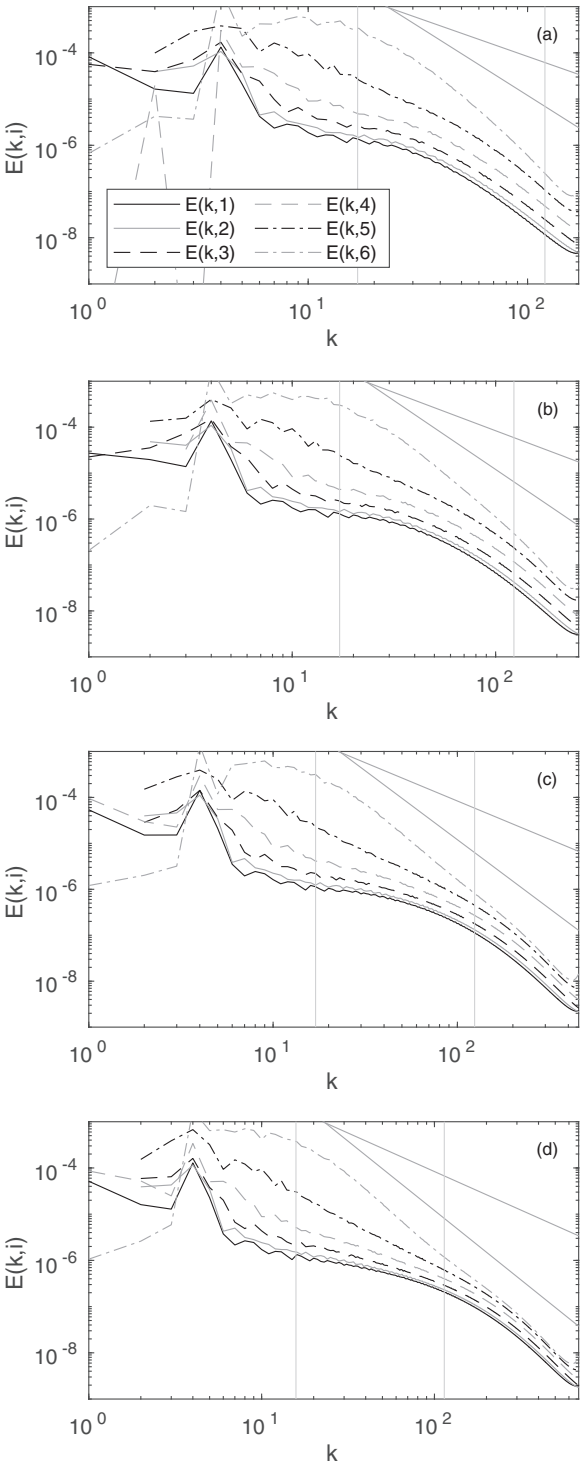

FIG. 9. Directional kinetic energy spectra for $N = 0.30$ for (a) $n = 384$, (b) 576, (c) 1024, and (d) 1536. In all cases, $k_b \approx 17$ and $k_O \approx 120$ are shown with vertical lines. The reference lines have slopes of $-5/3$ and -3.

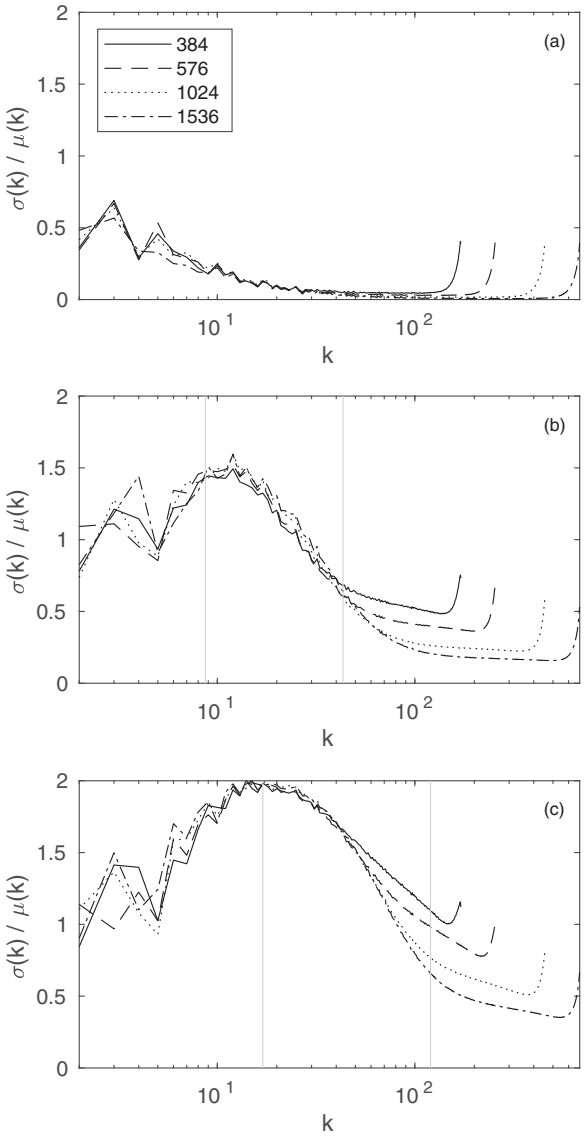

FIG. 10. Standard deviation of the directional spectra $E(k, i)$ over i, normalized by the mean, for (a) $N = 0$, (b) 0.15, and (c) 0.30. In the stratified cases (b) and (c), the buoyancy and Ozmidov wave numbers k_b and k_O, with $k_O > k_b$, are shown with vertical lines.

two values are similar to the Re_b estimates obtained above when considering χ_ϵ, but the last two are much larger.

E. Subfilter-scale dissipation

The relative contribution Π_{ij}/Π of the various components of the subfilter-scale dissipation are plotted in Fig. 13 for the four different filter cutoffs. At small Re_b for all filters, the subfilter-scale dissipation is dominated by the horizontal components Π_{11}, Π_{22}, and Π_{12}. The contribution from Π_{12} decreases when $k_c \geqslant k_O$ but is still larger than the vertical components. By contrast, the

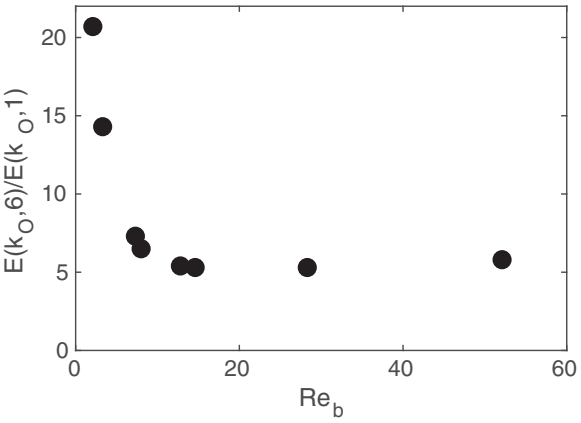

FIG. 11. Ratio of the Ozmidov-scale energy in $O_{k,6}$ to $O_{k,1}$.

behavior at larger Re_b, which appears to converge for $\mathrm{Re}_b \gtrsim 30$, is very sensitive to the scale of the filter. When the filter is imposed at scales larger than the Ozmidov scale [Figs. 13(a) and 13(b)], the Π_{ij} do not get more isotropic as Re_b increases; instead, the horizontal components continue to dominate even for $\mathrm{Re}_b = 50$, while $\Pi_{1,3}$, $\Pi_{2,3}$, and $\Pi_{3,3}$ are smaller than expected for isotropic turbulence. The anisotropy in the energy transfers above the Ozmidov scale, which are dominated by horizontal components, is different from that in viscous dissipation ϵ_{ij}, where vertical gradients dominated. This difference is due to the fact that vertical velocities and gradients, which influence the vertical components of Π_{ij} through τ_{ij} and $\tilde{s}_{ij}$, are inhibited above the Ozmidov scale in stratified turbulence.

As the cutoff wave number k_c crosses the Ozmidov wave number [Figs. 13(c) and 13(d)], Π_{ij} remains anisotropic at smaller Re_b as described above, with the horizontal terms dominating Π. However, as Re_b approach 20, the horizontal components decrease, and the vertical components increase, towards their isotropic values.

The overall approach to isotropy in the Π_{ij} and the dependence on Re_b can be seen in the mean square distance χ_Π in Fig. 14. For all filter scales, $\chi_\Pi \sim 10^{-2}$ for the smallest Re_b and decreases slightly as Re_b increases towards 10. Energy transfer through all of the filter scales becomes more

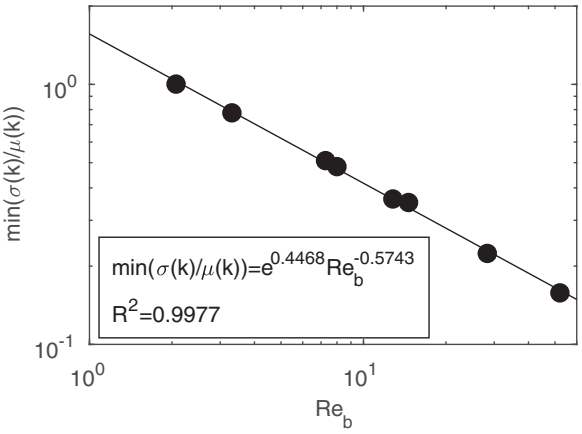

FIG. 12. The minimum value of $\sigma(k)/\mu(k)$ over k. All stratified simulations are included, and values are plotted vs Re_b. The solid line shows the power law best fit.

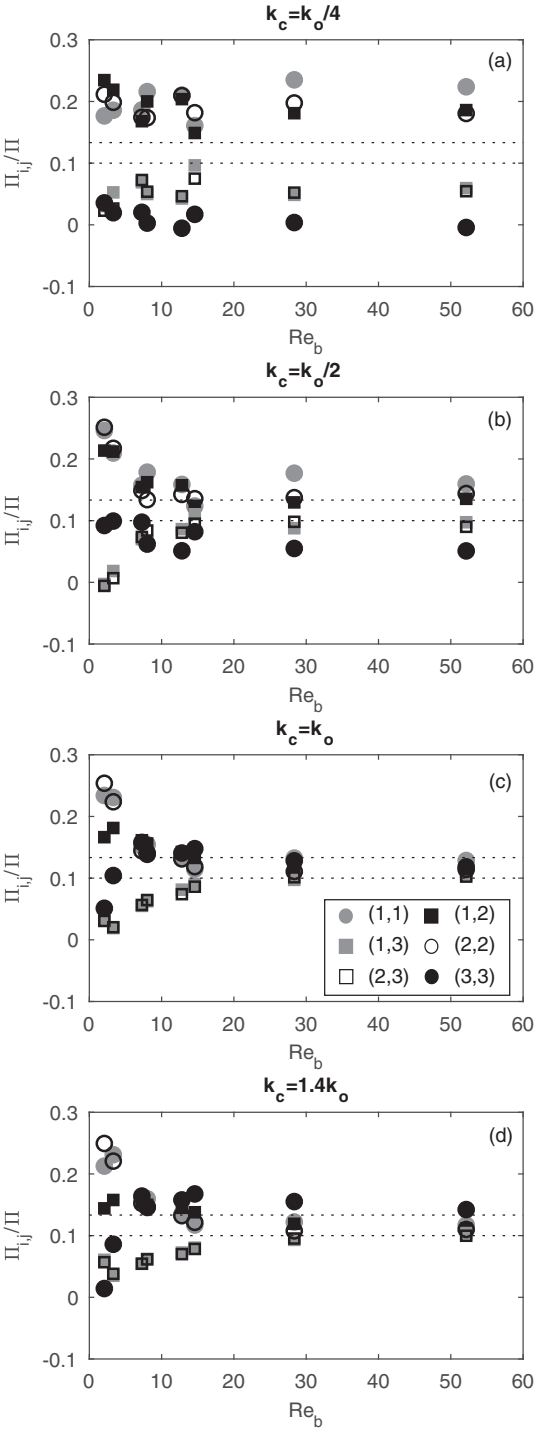

FIG. 13. Relative contribution of different components to the subfilter-scale dissipation Π_{ij}/Π for filter cutoff wave number $k_c =$ (a) $0.25k_O$, (b) $0.5k_O$, (c) k_O, and (d) $1.4k_O$. The isotropic values $1/10$ (for $i \neq j$) and $2/15$ (for $i = j$) are denoted by horizontal lines. All stratified simulations are included and values are plotted against Re_b.

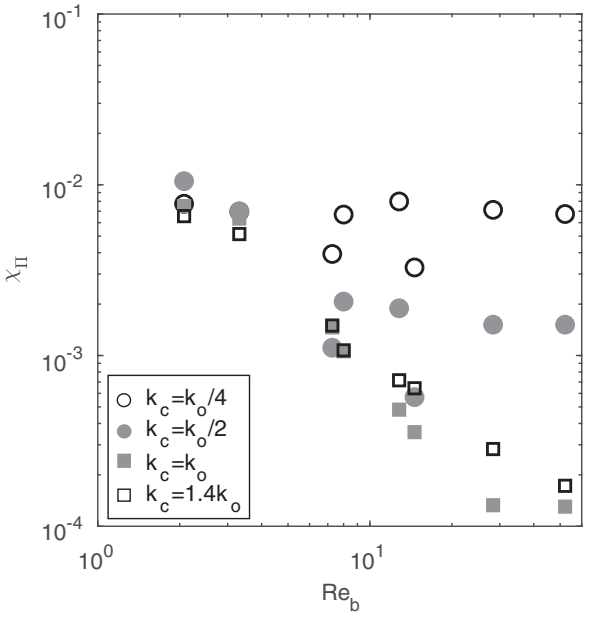

FIG. 14. Mean square distance χ_Π between the Π_{ij}/Π and their isotropic values.

isotropic as Re_b increases from 2, due to the reduction in viscous forces around the Ozmidov scale, as indicated by (4). The χ_Π values at small Re_b are similar to the χ_ϵ at the same Re_b. As Re_b increases beyond 7, the χ_Π values become more dependent on the filter used. At these intermediate $\mathrm{Re}_b \approx 10$, there is no collapse of the data with Re_b, even for a fixed filter scale (see, e.g., the spread in χ_Π for $k_c = k_O/4$ as Re_b increases from 8 to 15). However, the trend as Re_b increases towards 50 seems clear. For the largest scale filter $k_c/k_O = 1/4$, χ_Π plateaus at around 10^{-2} as Re_b increases to 50. The transfer of energy across $k_O/4$ is inherently anisotropic and does not become more isotropic with increasing Re_b. A similar behavior occurs for $k_c/k_O = 1/2$, for which χ_Π plateaus at around 2×10^{-3}. This plateau value is smaller than that obtained with $k_O/4$, indicating that the energy transfer across $k_O/2$ is more isotropic; however, transfer across this scale does not become more isotropic with increasing Re_b.

A different behavior occurs when the cutoff wave number is equal to or larger than the Ozmidov wave number. For $k_c/k_O = 1$ and 1.4, there is no plateau; instead, χ_Π generally decreases for increasing Re_b. The energy transfer across the Ozmidov scale does become increasingly isotropic as Re_b increases, in contrast to the transfers at larger scales. Larger Re_b implies a longer inertial range below the Ozmidov scale, which seems to enhance the isotropy at and below the Ozmidov scale.

V. CONCLUSIONS

We have performed direct numerical simulations to investigate the anisotropy of stratified turbulence and the transition to isotropy at small length scales. Turbulence was generated by forcing large-scale vortical modes, an approach that is broadly consistent with geophysical stratified turbulence, in which vortical (quasigeostrophic) motion dominates at large scales. The anisotropy of the turbulence at large scales, the Ozmidov scale, and small dissipation scales was quantified using four approaches: (1) the contributions of different strain rate components to the kinetic energy dissipation, which is a common isotropy diagnostic; (2) the invariants of the isotropy tensor and their position inside the Lumley triangle, which have not been widely applied to stratified turbulence, and which we couple with filtering to produce a scale-dependent isotropy measure; (3) directional

kinetic energy spectra, which provide a more complete picture of energy spectrum anisotropy than the more commonly used horizontal and vertical wave number spectra; and (4) the subfilter-scale energy flux, which we analyze in the same way as the dissipation. Together, these techniques offer a comprehensive picture of turbulence anisotropy across scales. We apply these techniques to stratified turbulence simulations with Re_b up to 50 and very strong stratification.

Isotropy at the dissipation scale increases with increasing Re_b, consistent with the interpretation of Re_b as the width of the inertial range between the Ozmidov and dissipation length scales. Significantly, the small-scale isotropy depends only on Re_b and not separately on Fr_h or Re. The singular importance of the parameter Re_b in characterizing the small-scale isotropy has been previously shown for the dissipation components [37]; we have demonstrated here that it also holds for the convergence of the directional spectra at small scales. Interestingly, the degree of isotropy in the dissipation components, and the spread of the directional spectra at small scales, all collapse to power laws when plotted against Re_b. These power laws can be extrapolated to estimate the degree of isotropy that will occur at even larger Re_b. While the threshold for what constitutes nearly isotropic is subjective, these quantities can be compared objectively to their values in unstratified turbulence at different Re. Interestingly, the extrapolation of both quantities indicates that $\mathrm{Re}_b \approx 500$ and 1000 are necessary for stratified turbulence to exhibit the same degree of small-scale isotropy found in the unstratified simulations with $\mathrm{Re} = 3000$ ($n = 384$) and $\mathrm{Re} = 5000$ ($n = 576$), respectively. These Re_b values are larger than that proposed in Ref. [27] (200) but smaller than that proposed in Ref. [37] for stratified shear flows (10^5). The small deviations from isotropy that occur at our largest Re_b are manifested as a slight bias towards vertical gradients in the dissipation and vertical wave numbers in the directional spectra.

Moving upscale towards the Ozmidov scale, the anisotropy increases. However, despite the definition of the Ozmidov scale as the transition scale at which buoyancy forces are always $O(1)$, the anisotropy at this scale may depend on Fr_h, Re, and Re_b. Different diagnostics offer different perspectives. The directional energy spectra start to diverge as k decreases towards k_O, as expected. For $\mathrm{Re}_b \gtrsim 10$, the spectra exhibit a fixed degree of anisotropy at the Ozmidov scale that does not change with increasing Re_b, Fr_h, or Re: the standard deviation in the spectra at k_O is approximately 0.7 in all such cases, and the ratio of kinetic energy in the most vertical and horizontal wave number bands is between 5 and 6. However, for smaller Re_b, viscous effects at the Ozmidov scale are non-negligible and there is more spread in the directional spectra around k_O. By contrast, the energy transfer across the Ozmidov wave number does become more isotropic for increasing Re_b, even for values $\gtrsim$10. Similarly, the invariants of the isotropy tensor at the Ozmidov scale, while generally much more isotropic than those at large scales, do become increasingly isotropic for increasing Fr_h and Re. Interestingly, the Ozmidov-scale invariants are not fully determined by Re_b and depend separately on Fr_h and Re. Overall, it appears that the energy transfer and invariants, which are both based on the Reynolds stresses at different length scales, are more sensitive to changes in anisotropy at the Ozmidov scale, likely because they include information from all scales below the cutoff. By contrast, the directional energy spectra, which describe the overall distribution of kinetic energy at specific wave numbers, see only a fixed degree of isotropy at the Ozmidov scale. Simulations with higher Re_b may be required to determine whether these different measures of Ozmidov-scale anisotropy converge as Re_b increases further.

Not surprisingly, the large scales display the most anisotropy, the degree of which is determined by Fr_h. The invariants of the isotropy tensor display significant anisotropy. All invariants lie on the axisymmetric curve that connects isotropic two- and three-dimensional turbulence; the invariants for $N = 0.3$ are located approximately half way between these extremes, while those for $N = 0.15$ are closer to the isotropic three-dimensional value. The large-scale invariants are set by Fr_h and are mostly independent of Re, consistent with the weak large-scale viscous effects in all these simulations.

The anisotropy of the directional spectra at large scales is demonstrated by a strong dependence on the wave vector angle: near-horizontal wave vectors have spectral slopes around -1 or shallower, while near-vertical wave vectors have slopes closer to -3 [54]. These spectra reduce

to approximately $k_h^{-5/3}$ when integrated in the vertical [8,9,15,19,22], but interestingly, only the directional spectra at intermediate angles ($i = 4$ or $\theta \in [\pi/4, \pi/3)$) have slopes around $-5/3$. At near-vertical wave vectors, where most of the energy is located, the peak is set by k_b rather than the forcing and is determined by Fr_h. Finally, the energy fluxes at scales larger than the Ozmidov scale, even at twice the Ozmidov scale, are inherently anisotropic and do not isotropize with increasing Re_b. The contrast in this behavior with that at $k \geqslant k_O$ underlines the importance of the Ozmidov scale in the transition to isotropy.

In summary, our simulations indicate the following trends in anisotropy at the three different scales of interest: Large-scale anisotropy is set by Fr_h and occurs at the buoyancy scale, associated with the thickness of the large-scale vortical modes. Stronger stratification leads to more large-scale anisotropy. Ozmidov-scale eddies are anisotropic. Energy spectra exhibit a fixed degree of anisotropy as Re_b increases, while the invariants and energy transfers become increasingly isotropic with increasing Fr_h and Re. Dissipation-scale isotropy is determined by Re_b. Our results suggest that $\mathrm{Re}_b \gtrsim 500$ is required to obtained the same degree of small-scale isotropy seen in unstratified turbulence at similar Re. The applicability of these findings to decaying stratified turbulence, and forced stratified turbulence in which the VSHF is allowed to grow to dominate the flow, requires further study.

These results have significant implications for the parametrization of subgrid turbulence in large eddy simulation of stratified turbulence. Most models assume isotropic subgrid turbulence, both through the use of three-dimensional eddy viscosity as well as through the particular eddy viscosity parametrization [55,56]. For grid spacings smaller than the Ozmidov scale, this assumption seems reasonable and, at a first approximation, is largely consistent with our results, especially for large Re_b, as there is a trend towards increased isotropy at the Ozmidov scale in this regime. On the other hand, isotropic models are inappropriate for much larger grid spacings and possibly questionable at the Ozmidov scale for modest Re_b. Any attempt to incorporate anisotropy into the subgrid model requires knowledge of how these effects depend on Fr_h, Re, and Re_b, which has been outlined here. While isotropic models have shown some promise with grid spacings around the buoyancy scale [55,56] (which is larger than the Ozmidov scale but, at least for numerical simulations, usually not much larger [9,21]), a subgrid modeling approach for strongly stratified turbulence with coarse grids, e.g., for geophysical flows, clearly requires an anisotropic treatment of the unresolved scales.

ACKNOWLEDGMENTS

This research was enabled in part by support provided by the Shared Hierarchical Academic Research Computing Network (SHARCNET) and Compute/Calcul Canada and funding from the Natural Sciences and Engineering Research Council of Canada (Grant No. RGPIN-386456-2015) and the Canadian Foundation for Innovation.

APPENDIX: ISOTROPIC VALUES OF Π_{ij}

To show that Π_{ij}/Π has the same values as ϵ_{ij}/ϵ for isotropic turbulence, we adapt Taylor's [52] derivation. For isotropic turbulence, the six independent terms of Π_{ij} can be written in terms of two independent values, one diagonal and one off-diagonal:

$$\Pi \equiv 2\langle \tau_{ij}\widetilde{s}_{ij}\rangle = 6\langle \tau_{11}\widetilde{s}_{11}\rangle + 12\langle \tau_{12}\widetilde{s}_{12}\rangle = 6\left\langle (\widetilde{u}^2 - \widetilde{u^2})\frac{\partial \widetilde{u}}{\partial x}\right\rangle + 12\left\langle (\widetilde{u}\widetilde{v} - \widetilde{u}\widetilde{v})\frac{\partial \widetilde{u}}{\partial y}\right\rangle. \tag{A1}$$

The filtered continuity equation gives

$$\frac{\partial \widetilde{u}}{\partial x} + \frac{\partial \widetilde{v}}{\partial y} + \frac{\partial \widetilde{w}}{\partial z} = 0, \tag{A2}$$

from which follows

$$\left\langle (\widetilde{u}^2 - \widetilde{u^2})\left(\frac{\partial \widetilde{u}}{\partial x} + \frac{\partial \widetilde{v}}{\partial y} + \frac{\partial \widetilde{w}}{\partial z}\right)\right\rangle = 0. \tag{A3}$$

Isotropy implies that

$$\left\langle (\widetilde{u}^2 - \widetilde{u^2})\left(\frac{\partial \widetilde{v}}{\partial y}\right)\right\rangle = \left\langle (\widetilde{u}^2 - \widetilde{u^2})\left(\frac{\partial \widetilde{w}}{\partial z}\right)\right\rangle, \tag{A4}$$

which, when substituted into (A3), gives

$$\left\langle (\widetilde{u}^2 - \widetilde{u^2})\left(\frac{\partial \widetilde{u}}{\partial x} + 2\frac{\partial \widetilde{v}}{\partial y}\right\rangle = 0. \tag{A5}$$

Now, consider a rotation of the coordinates by $\pi/4$ about the z axis, with new coordinates and velocities given by

$$\sqrt{2}x' = x + y, \quad \sqrt{2}y' = -x + y, \quad z' = z, \tag{A6}$$

$$\sqrt{2}u' = u + v, \quad \sqrt{2}v' = -u + v, \quad w' = w. \tag{A7}$$

By isotropy, we expect

$$\left\langle (\widetilde{u}^2 - \widetilde{u^2})\frac{\partial \widetilde{u}}{\partial x}\right\rangle = \left\langle (\widetilde{v'}^2 - \widetilde{v'^2})\frac{\partial \widetilde{v'}}{\partial y'}\right\rangle \tag{A8}$$

and

$$\left\langle (\widetilde{v}^2 - \widetilde{v^2})\frac{\partial \widetilde{v}}{\partial y}\right\rangle = \left\langle (\widetilde{u'}^2 - \widetilde{u'^2})\frac{\partial \widetilde{u'}}{\partial x'}\right\rangle \tag{A9}$$

which give, respectively,

$$\left\langle (\widetilde{u}^2 - \widetilde{u^2})\frac{\partial \widetilde{u}}{\partial x}\right\rangle = \frac{1}{4}\left\langle (\widetilde{u}^2 - 2\widetilde{u}\,\widetilde{v} + \widetilde{v}^2 - \widetilde{u^2} + 2\widetilde{uv} - \widetilde{v^2})\left(\frac{\partial \widetilde{u}}{\partial x} - \frac{\partial \widetilde{u}}{\partial y} - \frac{\partial \widetilde{v}}{\partial x} + \frac{\partial \widetilde{v}}{\partial y}\right)\right\rangle, \tag{A10}$$

and

$$\left\langle (\widetilde{v}^2 - \widetilde{v^2})\frac{\partial \widetilde{v}}{\partial y}\right\rangle = \frac{1}{4}\left\langle (\widetilde{u}^2 + 2\widetilde{u}\,\widetilde{v} + \widetilde{v}^2 - \widetilde{u^2} - 2\widetilde{uv} - \widetilde{v^2})\left(\frac{\partial \widetilde{u}}{\partial x} + \frac{\partial \widetilde{u}}{\partial y} + \frac{\partial \widetilde{v}}{\partial x} + \frac{\partial \widetilde{v}}{\partial y}\right)\right\rangle. \tag{A11}$$

Summing (A10) and (A11) and using, by the assumption of isotropy, that

$$\left\langle (\widetilde{v}^2 - \widetilde{v^2})\frac{\partial \widetilde{v}}{\partial y}\right\rangle = \left\langle (\widetilde{u}^2 - \widetilde{u^2})\frac{\partial \widetilde{u}}{\partial x}\right\rangle, \tag{A12}$$

leads to

$$\left\langle (\widetilde{u}^2 - \widetilde{u^2})\left(\frac{\partial \widetilde{u}}{\partial x} - \frac{\partial \widetilde{v}}{\partial y}\right)\right\rangle = 2\left\langle (\widetilde{u}\,\widetilde{v} - \widetilde{uv})\frac{\partial \widetilde{u}}{\partial y}\right\rangle. \tag{A13}$$

Substituting into (A5) and simplifying, we find that

$$\left\langle (\widetilde{u}\,\widetilde{v} - \widetilde{uv})\frac{\partial \widetilde{u}}{\partial y}\right\rangle = \frac{3}{4}\left\langle (\widetilde{u}^2 - \widetilde{u^2})\frac{\partial \widetilde{u}}{\partial x}\right\rangle, \tag{A14}$$

and therefore, from (A1),

$$\Pi = \frac{15}{2}\left\langle (\widetilde{u}^2 - \widetilde{u^2})\frac{\partial \widetilde{u}}{\partial x}\right\rangle. \tag{A15}$$

Consider the expressions for the diagonal and off-diagonal components of Π_{ij}. If $i = j$, then

$$\Pi_{ij} = \left\langle (\widetilde{u}^2 - \widetilde{u^2}) \frac{\partial \widetilde{u}}{\partial x} \right\rangle. \tag{A16}$$

If $i \neq j$, then

$$\Pi_{ij} = \left\langle (\widetilde{u}\,\widetilde{v} - \widetilde{uv}) \frac{\partial \widetilde{u}}{\partial y} \right\rangle = \frac{3}{4} \left\langle (\widetilde{u}^2 - \widetilde{u^2}) \frac{\partial \widetilde{u}}{\partial x} \right\rangle. \tag{A17}$$

From (A15), we see that

$$\frac{\Pi_{ij}}{\Pi} = \begin{cases} \frac{2}{15} & i = j \\ \frac{1}{10} & i \neq j \end{cases}. \tag{A18}$$

So, for isotropic turbulence, the relative contributions of the different Π_{ij} to Π are the same as the contributions of the different ϵ_{ij} to the molecular dissipation (12).

[1] J. J. Riley and M.-P. Lelong, Fluid motions in the presence of strong stable stratification, Annu. Rev. Fluid Mech. **32**, 613 (2000).

[2] J. J. Riley and E. Lindborg, Stratified turbulence, in *Ten Chapters in Turbulence*, edited by P. A. Davidson, Y. Kaneda, and K. R. Sreenivasan (Cambridge University Press, Cambridge, 2013), p. 269.

[3] P. A. Davidson, *Turbulence in Rotating, Stratified and Electrically Conducting Fluids* (Cambridge University Press, Cambridge, 2013).

[4] J. J. Riley and E. Lindborg, Stratified turbulence: A possible interpretation of some geophysical turbulence measurements, J. Atmos. Sci. **65**, 2416 (2008).

[5] J. R. Herring and O. Métais, Numerical experiments in forced stably stratified turbulence, J. Fluid Mech. **202**, 97 (1989).

[6] J. J. Riley and S. M. deBruynKops, Dynamics of turbulence strongly influenced by buoyancy, Phys. Fluids **15**, 2047 (2003).

[7] M. L. Waite and P. Bartello, Stratified turbulence dominated by vortical motion, J. Fluid Mech. **517**, 281 (2004).

[8] E. Lindborg, The energy cascade in a strongly stratified fluid, J. Fluid Mech. **550**, 207 (2006).

[9] G. Brethouwer, P. Billant, E. Lindborg, and J.-M. Chomaz, Scaling analysis and simulation of strongly stratified turbulent flows, J. Fluid Mech. **585**, 343 (2007).

[10] P. Augier, P. Billant, and J.-M. Chomaz, Stratified turbulence forced with columnar dipoles: Numerical study, J. Fluid Mech. **769**, 403 (2015).

[11] J. J. Riley, R. W. Metcalfe, and M. A. Weissman, Direct numerical simulations of homogeneous turbulence in density-stratified fluids, AIP Conf. Proc. **76**, 79 (1981).

[12] D. K. Lilly, Stratified turbulence and the mesoscale variability of the atmosphere, J. Atmos. Sci. **40**, 749 (1983).

[13] M.-P. Lelong and J. J. Riley, Internal wave-vortical mode interactions in strongly stratified flows, J. Fluid Mech. **232**, 1 (1991).

[14] P. Billant and J.-M. Chomaz, Self-similarity of strongly stratified inviscid flows, Phys. Fluids **13**, 1645 (2001).

[15] A. Maffioli and P. A. Davidson, Dynamics of stratified turbulence decaying from a high buoyancy Reynolds number, J. Fluid Mech. **786**, 210 (2016).

[16] J.-P. Laval, J. C. McWilliams, and B. Dubrulle, Forced stratified turbulence: Successive transitions with Reynolds number, Phys. Rev. E **68**, 036308 (2003).

[17] M. L. Waite, Stratified turbulence at the buoyancy scale, Phys. Fluids **23**, 066602 (2011).

[18] F. S. Godeferd and C. Staquet, Statistical modeling and direct numerical simulations of decaying stably stratified turbulence. Part 1. Flow energetics, J. Fluid Mech. **360**, 295 (1998).
[19] P. Bartello and S. Tobias, Sensitivity of stratified turbulence to the buoyancy Reynolds number, J. Fluid Mech. **725**, 1 (2013).
[20] S. Khani and M. L. Waite, Effective eddy viscosity in stratified turbulence, J. Turbul. **14**, 49 (2013).
[21] M. L. Waite, Direct numerical simulations of laboratory-scale stratified turbulence, in *Modelling Atmospheric and Oceanic Flows: Insights from Laboratory Experiments and Numerical Simulations*, edited by T. von Larcher and P. D. Williams (American Geophysical Union, 2013), p. 159.
[22] Y. Kimura and J. R. Herring, Energy spectra of stably stratified turbulence, J. Fluid Mech. **698**, 19 (2012).
[23] F. S. Godeferd, A. Delache, L. Gostiaux, and C. Cambon, A multiscale point of view on the dynamics of stably stratified turbulence associated with geostrophic modes: simulations and model, in *Proc. 8th International Symposium on Stratified Flows* (Scripps Institution of Oceanography, University of California San Diego, 2016).
[24] J. P. Dougherty, The anisotropy of turbulence at the meteor level, J. Atmos. Terr. Phys. **21**, 210 (1961).
[25] R. V. Ozmidov, On the turbulent exchange in a stably stratified ocean, Bull. (Ivz.) Acad. Sci. USSR, Atmos. Ocean. Phys. **1**, 493 (1965).
[26] A. E. Gargett, P. J. Hendricks, T. B. Sanford, T. R. Osborn, and A. J. Williams III, A composite spectrum of vertical shear in the upper ocean, J. Phys. Oceanogr. **11**, 1258 (1981).
[27] A. E. Gargett, T. R. Osborn, and P. W. Nasmyth, Local isotropy and the decay of turbulence in a stratified fluid, J. Fluid Mech. **144**, 231 (1984).
[28] E. Kunze, A unified model spectrum for anisotropic stratified and isotropic turbulence in the ocean and atmosphere, J. Phys. Oceanogr. **49**, 385 (2019).
[29] S. Almalkie and S. M. de Bruyn Kops, Kinetic energy dynamics in forced, horizontally homogeneous and isotropic, stably stratified turbulence, J. Turbul. **13**, N29 (2012).
[30] P. Augier, J.-M. Chomaz, and P. Billant, Spectral analysis of the transition to turbulence from a dipole in stratified fluids, J. Fluid Mech. **713**, 167 (2012).
[31] T. M. Dillon and D. R. Caldwell, The Batchelor spectrum and dissipation in the upper ocean, J. Geophys. Res. **85**, 1910 (1980).
[32] A. Pouquet, D. Rosenberg, R. Marino, and C. Herbert, Scaling laws for mixing and dissipation in unforced rotating stratified turbulence, J. Fluid Mech. **844**, 519 (2018).
[33] C. H. Gibson, Fossil temperature, salinity, and vorticity turbulence in the ocean, in *Marine Turbulence*, edited by J. C. J. Nihoul (Elsevier, 1980).
[34] E. C. Itsweire, J. R. Koseff, D. A. Briggs, and J. H. Ferziger, Turbulence in stratified shear flows: Implications for interpreting shear-induced mixing in the ocean, J. Phys. Oceanogr. **23**, 1508 (1993).
[35] C. R. Rehmann and J. H. Hwang, Small-scale structure of strongly stratified turbulence, J. Phys. Oceanogr. **35**, 151 (2005).
[36] D. A. Hebert and S. M. de Bruyn Kops, Relationship between vertical shear rate and kinetic energy dissipation rate in stably stratified flows, Geophys. Res. Lett. **33**, L06602 (2006).
[37] W. D. Smyth and J. N. Moum, Anisotropy of turbulence in stably stratified mixing layers, Phys. Fluids **12**, 1343 (2000).
[38] A. M. Fincham, T. Maxworthy, and G. R. Spedding, Energy dissipation and vortex structure in freely decaying, stratified grid turbulence, Dyn. Atmos. Oceans **23**, 155 (1996).
[39] F. S. Godeferd and C. Staquet, Statistical modeling and direct numerical simulations of decaying stably stratified turbulence. Part 2. Large-scale and small-scale anisotropy, J. Fluid Mech. **486**, 115 (2003).
[40] O. Praud, A. M. Fincham, and J. Sommeria, Decaying grid turbulence in a strongly stratified fluid, J. Fluid Mech. **522**, 1 (2005).
[41] S. de Bruyn Kops, Classical scaling and intermittency in strongly stratified Boussinesq turbulence, J. Fluid Mech. **775**, 436 (2015).
[42] J. L. Lumley and G. R. Newman, The return to isotropy of homogeneous turbulence, J. Fluid Mech. **82**, 161 (1977).
[43] S. B. Pope, *Turbulent Flows* (Cambridge University Press, Cambridge, 2000).
[44] S. Khani and M. L. Waite, Backscatter in stratified turbulence, Eur. J. Mech. B Fluids **60**, 1 (2016).

[45] D. R. Durran, *Numerical Methods for Wave Equations in Geophysical Fluid Dynamics* (Springer, Berlin, 1999).
[46] M. L. Waite, Random forcing of geostrophic motion in rotating stratified turbulence, Phys. Fluids **29**, 126602 (2017).
[47] M. L. Waite and P. Bartello, Stratified turbulence generated by internal gravity waves, J. Fluid Mech. **546**, 313 (2006).
[48] L. M. Smith and F. Waleffe, Generation of slow large scales in forced rotating stratified turbulence, J. Fluid Mech. **451**, 145 (2002).
[49] C. Herbert, R. Marino, D. Rosenberg, and A. Pouquet, Waves and vortices in the inverse Cascade regime of stratified turbulence with or without rotation, J. Fluid Mech. **806**, 165 (2016).
[50] J. G. Fitzgerald and B. F. Farrell, Statistical state dynamics of vertically sheared horizontal flows in two-dimensional stratified turbulence, J. Fluid Mech. **854**, 544 (2018).
[51] S. M. de Bruyn Kops and J. J. Riley, The effects of stable stratification on the decay of initially isotropic homogeneous turbulence, J. Fluid Mech. **860**, 787 (2019).
[52] G. I. Taylor, Statistical theory of turbulence, Proc. R. Soc. London, Ser. A **151**, 421 (1935).
[53] A. Delache, C. Cambon, and F. Godeferd, Scale by scale anisotropy in freely decaying rotating turbulence, Phys. Fluids **26**, 025104 (2014).
[54] A. Maffioli, Vertical spectra of stratified turbulence at large horizontal scales, Phys. Rev. Fluids **2**, 104802 (2017).
[55] S. Khani and M. L. Waite, Buoyancy scale effects in large-eddy simulations of stratified turbulence, J. Fluid Mech. **754**, 75 (2014).
[56] S. Khani and M. L. Waite, Large eddy simulations of stratified turbulence: The dynamic Smagorinsky model, J. Fluid Mech. **773**, 327 (2015).